Grazing incidence echelle spectrometers using varied line-space gratings

Michael C. Hettrick

Applied Optics Vol. 24, Issue 9, pp. 1251-1255 (1985)

http://dx.doi.org/10.1364/AO.24.001251

Grazing incidence echelle spectrometers using varied line-space gratings

Michael C. Hettrick

Creative Optics, 1510-F Bonita Avenue, Berkeley, California 94709.
Received 11 January 1985.
0003-6935/85/091251-05$02.00/0.

High resolution spectrometers operating in the soft x ray (10–100 Å) and extreme ultraviolet (100–1000 Å) have recently become a subject of much interest.[1–11] A variety of designs can be found which meet the requirements of specific experiments. However, a general approach to this problem would ideally result in a design which not only delivers high spectral resolution but also meets several other generic goals including high efficiency, low background, and a wide instantaneous spectrum.

We have previously suggested a new two-element echelle spectrometer[12,13] composed of varied line-space (VLS) gratings at grazing incidence. The absence of other correcting or collimating/camera optics permits high reflection efficiency in comparison to standard approaches. In combination with a two-element grazing incidence telescope,[14] a sample design for use in space astronomy has been calculated to deliver an optics efficiency greater than 5%. In this Letter we provide quantitative estimates of the imaging performance expected from a VLS echelle spectrometer.

In Fig. 1 we show two versions of the proposed design. Each features a fan grating[12] or radial groove grating[15] as the high-dispersion echelle. To achieve high resolution, this radial–fan must be ruled with varied angular spacings.[13] The extreme off-plane mounting, shown in Fig. 2, results in high peak blaze efficiency[16,17] and a constant blazed wavelength across the grating aperture.[12] An additional advantage stems from a general focusing condition of the fan,[13] whereby a judicious placement of the ruling focus results in optimized imaging of all incident foci lying along a circle or sphere connecting the grating center and the ruling focus.

The echelle is preceded by a concentric groove grating[12,13] which functions as the cross disperser. This results in a correction to the echelle-blazed wavelengths. Between adjacent orders $(m,m+1)$, these will be separated by

$$\lambda_m - \lambda_{m+1} = \lambda_m/m/(1 - \lambda_m/r/p_c), \tag{1}$$

where p_c is the disperser plate scale and r is the radius of the echelle dispersion cone (see Fig. 2). While typically not a serious design constraint, the choice of sign for p_c can provide either more tightly packed echelle orders ($p_c < 0$) or more separated but longer orders ($p_c > 0$). In Eq. (1) a positive plate scale signifies that longer wavelengths strike the echelle at larger graze angles.

Regardless of this correction factor, a useful property of the fan grating is that the blazed wavelength is nearly constant for all regions of the grating aperture. For a uniform blaze angle, the blazed wavelength shifts only by a fraction $\sim \gamma_e/f_{ex}$, where γ_e is the mean graze angle and f_{ex} is the beam speed along the groove lengths. This permits the fan to operate efficiently in spectral orders $m \lesssim f_{ex}/\gamma_e$.

Each of the two gratings can be fabricated by mechanical ruling[18,19] resulting in triangular groove shapes which deliver high groove efficiencies.[20,21] The gratings are configured geometrically to accept converging light and to image the diffracted waves on a common focal surface. The detecting surface is illuminated at an angle of incidence γ_e equal to the mean graze angle striking the echelle. Thus for grazing echelle angles, the detector is operated at nearly normal incidence.

A Type I design version [Fig. 1(a)] provides near-coincidence of the echelle focal surface with the tangential foci of the disperser, which lie along a curve with a radius less than $L_c/2$, where L_c is the mean distance from the disperser to focus.[13] The physical layout of this design is compact, where the spectrum lies near the incident focus. However, the disperser broadens its images in the direction of the echelle dispersion by an amount proportional to the displacement of the tangential and sagittal foci. If their loci are approximated by planes in the vicinity of the aberration-corrected wavelength λ_* where they intersect at an angle τ, the image is broadened by

$$\Delta b = \tau|\lambda - \lambda_*|/p_c/f_{cy}, \tag{2}$$

where f_{cy} is the speed of the beam incident to the disperser along its grooves. In the Type I configuration, τ equals the sum of the disperser and echelle graze angles.

In Fig. 1(b) we show an alternate Type II configuration in which the echelle focal surface coincides with the symmetry axis of the concentric grooves, along which the above-mentioned image broadening vanishes for all wavelengths.[12] If not for the image rotation induced by the conical echelle,[6,22] this would be the clear choice for maximum wavelength discrimination in the high-dispersion direction. The Type II design also provides a convenient geometry for which to estimate system performance due to the near decoupling of aberrations for each grating.

Aberrations of the individual gratings have been presented previously.[13] For the varied-angle fan echelle, the aberrant light-path distance is

$$\Delta = (m\lambda_*/d_e)[\tfrac{1}{2}\gamma_e^2(x^2y + y^3) - \tfrac{1}{8}(m\lambda_*/d_e)^2y^3 + \ldots], \tag{3}$$

where m is the spectral order, d_e is the nominal line spacing, x is measured along the grooves, y is measured across the ruled width, and all distances are in units of the mean distance L_e from echelle to focus. The resultant image is traced according to the equations

$$a = (\partial\Delta/\partial x)/\sin\gamma_e, \quad b = (\partial\Delta/\partial y)/\cos\delta - a\tan\delta, \tag{4}$$

where a is the image height coordinate, b is in the echelle dispersion direction, and δ is the echelle blaze angle. As the echelle is mounted in the extreme off-plane (Fig. 2), δ equals the common angle of incidence and diffraction. We show in Fig. 3(a) the image envelope in the limit as δ vanishes, for rays which trace the periphery and diagonals of a rectangular grating aperture. The maximum image width is along $a = 0$ and yields a grating spectral resolution[13]

$$\lambda/\Delta\lambda = 8 \cdot \min(f_{ex}^2, \tfrac{2}{3}f_{ey}^2/\gamma_e^2/\cos^2\delta). \tag{5a}$$

In Fig. 3(a) we have shown the usual case where this resolution is determined by the f_{ex} term ($f_{ex} = 40, f_{ey} = 20, \gamma_e = 12.5°$). The term in f_{ey} can be removed by a slight modification to the groove angular spacings. If these spacings are $\Delta\theta \propto 1 + \eta\theta^2$, then $\eta = \frac{1}{2}(1 + 3\gamma_e^2\cos^2\delta)$ is the modified space variation as derived from the c_{03} entry in Table I of Ref. 13 where we have substituted the blaze condition $m\lambda_*/d_e = 2\sin\delta\sin\gamma_e$. In either case, the image heights are[13]

$$\Delta a = (L_e/2)(m\lambda_*/d_e)/f_{ex}/f_{ey}, \tag{5b}$$

In Fig. 3(b) we show the image shape resulting from a large blaze angle, $\delta = 45°$. The image rotates by an equal amount and thus its height aligns with the grating normal independent of δ. Although the spectral resolution does not degrade as a result, the required detector resolution increases by $\cos\delta$.

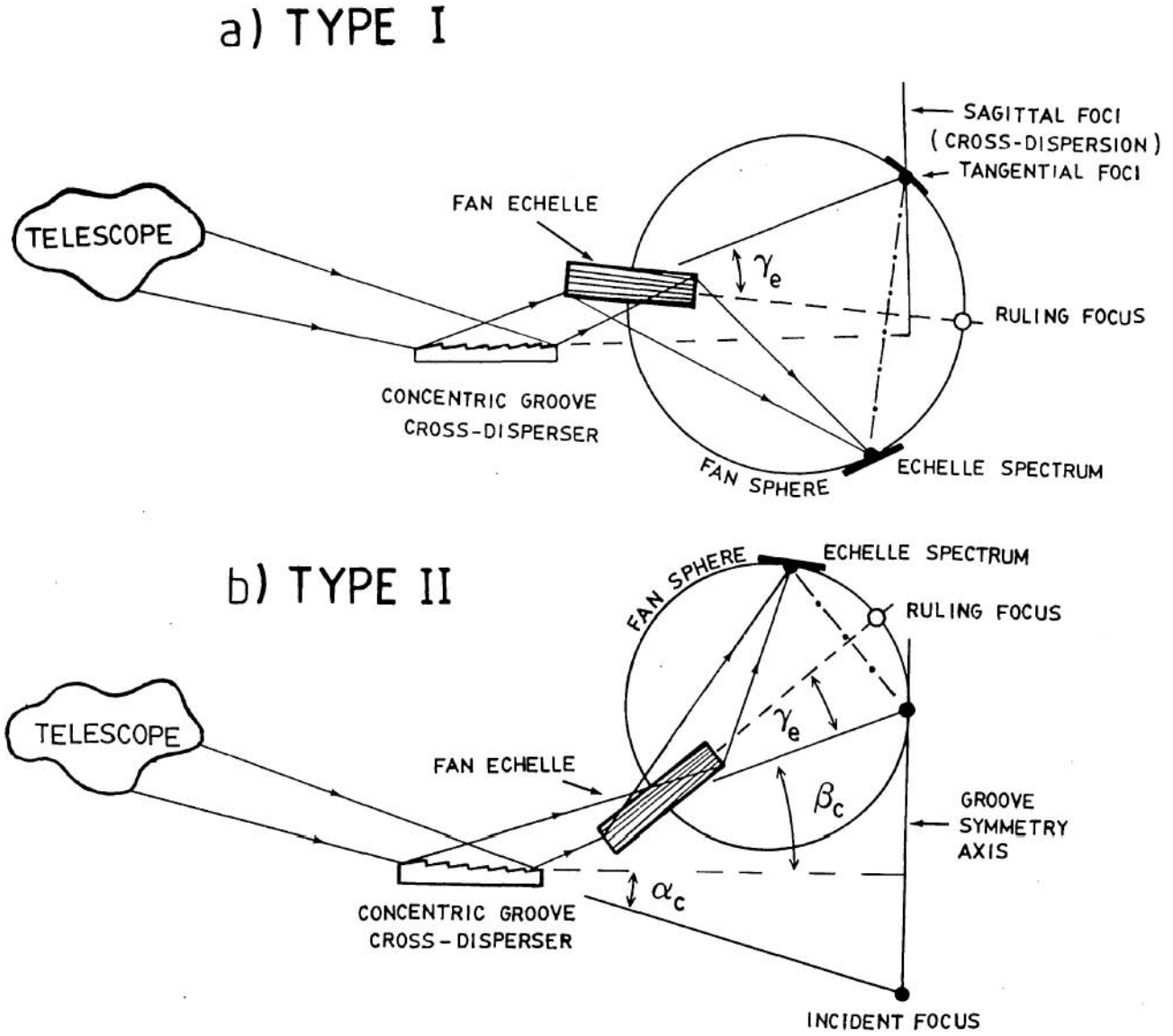

Fig. 1. Varied line-spacing echelle spectrometers. A telescope or other optic provides convergent light incident to two plane gratings. The cross disperser diffracts within the plane of this figure. The off-plane mounted echelle reflects blazed orders within this plane; the echelle normal is therefore tilted out of the figure plane by the (large) blaze angle of its grooves which are seen here in projection. The echelle disperses perpendicular to the figure plane and along a cone which intersects the fan sphere in a detecting circle whose plane is shown by the dot–dash line. The optimum detector is tilted relative to this plane about the echelle normal. A plane detector is shown extended in the direction of cross dispersion and is illuminated at an angle γ_e to its normal.

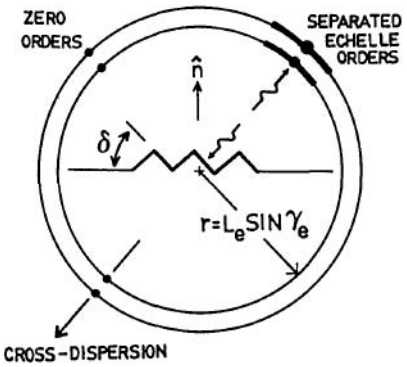

Fig. 2. Projection of echelle diffraction cone on the (sagittal) detecting plane normal to the central groove. The centers of each echelle order are perfectly blazed. Each order m extends to the blazed wavelengths of adjacent orders $(m-1, m+1)$. The cross-disperser grating changes the echelle cone radius r as a function of wavelength.

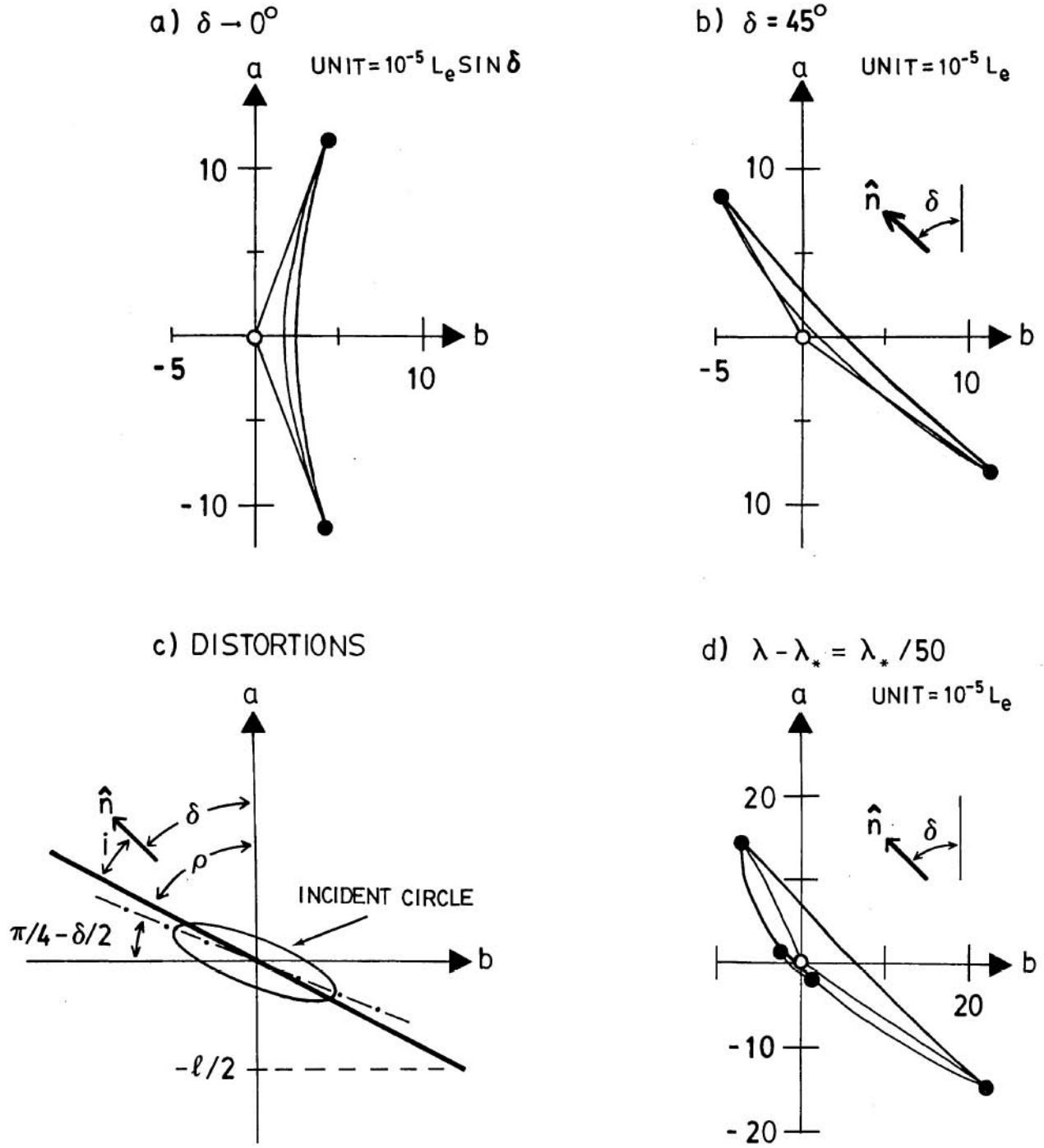

Fig. 3. Spot diagrams produced by an $f40 \times f20$ varied-angle fan grating illuminated at a 12.5° graze angle. Horizontal axis is in the dispersion direction: (a) ray trace in the limit as the blaze angle vanishes; the open circle corresponds to the grating center and the solid circles correspond to the grating corners; (b) ray trace for a 45° blaze angle ($\hat{n}$ is in the direction of the grating normal); (c) image distortions induced by the 45° echelle; the dot–dash line is the major axis of the elliptical image from an incident circle; the heavy line is the diffracted image of a vertical line with height l; (d) same as (b) but at $\lambda = \lambda_* + \lambda_*/50$.

Accompanying the ray traces is Fig. 3(c) showing the elliptical image produced by the echelle's distortion of an incident blur circle having equal enclosed area. In isolation the circle or ellipse determines a dispersive limit to the spectral resolution

$$\Delta\lambda_{disp}/\lambda = \Delta\phi/\tan\delta/\sin\gamma_e, \quad (6)$$

where $\Delta\phi$ is the radius of the incident circle relative to L_e. If the incident converging light is provided by a telescope with focal length F and image quality ε, then $\Delta\phi = \frac{1}{2}(F/L_e)\varepsilon$. A summation in quadrature with the echelle extremum aberration then yields a conservative subtotal value for the system resolution. To this we must convolve the cross-disperser aberration[13]

$$l = 3W(m\lambda/d_c)^2|1 - \lambda_*/\lambda|/\sin\alpha_c, \quad (7)$$

where d_c is the disperser nominal line spacing, W is its ruled width, and α_c is the nominal graze angle of incidence. This image is equivalent to an infinitely thin slit with length l perpendicular to echelle dispersion. However after diffraction this slit is elongated and rotated by an angle $\rho = \arctan(2\tan\delta\cos\gamma_e)$ as shown in Fig. 3(c) and given in Ref. 6. Except for $\delta = 0$ or $\delta = 90°$, this rotated slit will not lie in the same major direction as the echelle grating aberrations. The included angle i determines the degraded spectral resolution

$$\Delta\lambda_{\text{total}} \simeq \Delta\lambda'[1 + (l/\Delta b)\sin i/\cos\rho], \quad l > 2L_e\Delta\phi, \quad (8)$$

where $\Delta\lambda'$ is the resolution subtotaled above and Δb is the image width corresponding to that resolution. We find the term $i = \arctan(2\tan\delta\cos\gamma_e) - \delta$ is bounded for all angles δ, $0 < \sin i < \frac{1}{3}$, reaching the maximum for $\delta \simeq 35°$. Thus if l is kept below Δb, the resolution at the edges of the cross dispersion degrades by at most ~40%. Equation (8) treats each grating aberration independently and therefore does not include possible cancellation of these errors through cross talk between the grating apertures.

A final consideration is the echelle aberration away from the blazed wavelengths given by Eq. (1). If one uses the sagittal plane of Fig. 2 (also dot–dash line in Fig. 1), the aberrant light-path distance will include a large term in y^2 resulting in severe degradation of spectral resolution. Use of the tangential focus, a cylinder,[13] will remove this term. Given that the echelle is used only near blaze, this cylinder is well approximated by a plane tilted toward the ruling focus by an angle μ about the grating normal:

$$\mu = \arctan(m\lambda_*/d_e) = \arctan(2\sin\gamma_e\sin\delta). \quad (9)$$

If each echelle order is extended to the blazed wavelength of adjacent orders [Eq. (1)], the wavelength-field aberration is

$$(\Delta\lambda/\lambda)_{\text{edge}} \simeq (m\lambda_*/d_e)(m\lambda/d_e)/(m\gamma_e f_{ex})/(1 - \lambda/r/p_c). \quad (10)$$

In Fig. 3(d) we show the ray trace corresponding to Fig. 3(b) but taken at the edge of spectral order $m = 50$. In agreement with Eq. (10), the spectral resolution has degraded to equal only ~40% of its value at λ_*.

We conclude with a numerical example which illustrates the capabilities of the proposed design. Consider an incident beam with $f_{ex} = 40$ and $f_{ey} = 40$, and an incident blur circle radius $\Delta\phi = 1$ sec of arc. We seek to obtain a resolution $\lambda/\Delta\lambda = 30{,}000$ simultaneously over a 30% spectral band from 228 to 304 Å. To reduce the echelle aberration at $\lambda_* = 266$ Å below $\Delta\lambda/\lambda = 2 \times 10^{-5}$ we split the echelle into two halves, each 400 mm long and each accepting $f_{ex} = 80$ along the grooves. With a graze angle $\gamma_e = 12.5°$, Eq. (6) determines that a blaze angle of $\delta = 45°$ will result in a dispersive contribution of 2.3×10^{-5} to the wavelength resolution. In quadrature, the above two terms yield a fractional wavelength resolution of 3×10^{-5}. The actual resolution will be somewhat better since Eq. (5a) overestimates the image full width at half-maximum. Given $L_e = 2500$ mm, the echelle plate scale is 0.21–0.28 Å/mm resulting in an image width of $\Delta b = 25$ μm. Because the echelle grating aberration dominates the image shape, its distortion by 45° [see Fig. 3(b)] results in a minor dimension of ~18 μm. Thus, a detector resolution of 10 μm, summed in quadrature, will degrade the spectral resolution by only ~10%. From Eq. (5b), the image heights perpendicular to dispersion are 0.12 mm. Using a detector of 25-mm diameter, the cross-dispersion plate scale is 3 Å/mm. A disperser distance $L_c = 3000$ mm and graze angle of 12.5° require a 350-mm ruled width and a nominal line density of 240 mm^{-1}. From Eq. (7) the disperser aberration rises to 30 μm at the spectrum edges which from Eq. (8) degrades the spectral resolution by 40% to $\lambda/\Delta\lambda = 24{,}000$. Using Eq. (10) we find that echelle orders greater than 165 are required to maintain a resolution of 30,000 at the edges of an echelle order. Order 165 (near 304 Å) extends to 13 mm in full width, and order 220 (near 228 Å) extends to 10 mm in full width. The minimum spacing between echelle orders is 0.33 mm, approximately three times the 0.12-mm thickness of each order. The detector area enclosed by an individual image is only ~3 $\times 10^{-5}$ cm^2, which contains very small levels of background (a typical background rate is 1 count/sec/cm^2).

A relaxation of the resolution requirement to $\lambda/\Delta\lambda = 10^4$ allows a significantly wider spectral band. For example, an $f40 \times f20$ beam can be imaged with this resolution instantaneously from 100 to 300 Å on a 50-mm diam detector having rectangular pixels of 15 × 100 μm. Extension to shallower graze angles and hence to x-ray wavelengths is also possible. For example, using an $f100 \times f20$ incident beam and a 3° graze angle, a resolution of $\lambda/\Delta\lambda = 5000$ is attainable over the 8–25-Å band. These various designs have potential applications in both laboratory and space experiments.

References

1. D. L. Garrett and R. Tousey, "Solar XUV Grazing Incidence Spectrograph on Skylab," Appl. Opt. **16,** 898 (1977).
2. S. O. Kastner and C. Wade, Jr., "Aspheric Grating for Extreme Ultraviolet Astronomy," Appl. Opt. **17,** 1252 (1978).
3. D. D. Dietrich, R. J. Fortner, D. F. Price, R. E. Stewart, C. Gilman, and H. Helave, "Development of a Temporally and Spatially Resolved Grazing Incidence Spectrometer," High-Temperature Plasma Diagnostics Conference, Los Angeles (Mar. 1980).
4. R. J. Fonck, A. T. Ramsey and R. V. Yelle, "Multichannel Grazing-Incidence Spectrometer for Plasma Impurity Diagnosis: SPRED," Appl. Opt. **21,** 2115 (1982).
5. E. Kallne, "New Approaches in Analysis of Soft X-Rays Using Gratings," Nucl. Instrum. Methods **195,** 105 (1982).
6. W. Cash, "Echelle Spectrographs at Grazing Incidence," Appl. Opt. **21,** 710 (1982).
7. W. E. McClintock and W. Cash, "Grazing Incidence Optics: New Techniques for High Sensitivity Spectroscopy in the Space Ultraviolet," Proc. Soc. Photo-Opt. Instrum. Eng. **331,** 321 (1982).
8. T. Kita, T. Harada, N. Nakano, and H. Kuroda, "Mechanically Ruled Aberration-Corrected Concave Gratings for a Flat-Field Grazing-Incidence Spectrograph," Appl. Opt. **22,** 512 (1983).
9. M. Pouey, "New Grazing Incidence Spectrometer for Hot Plasma Diagnostics," J. Phys. **44,** C8–201 (1983).
10. W. Werner and H. F. van Beek, "Grazing Incidence Focal Plane Instrument for the Wavelength Range 6.5–175 nm," Proc. Soc. Photo-Opt. Instrum. Eng. **445,** 272 (1983).
11. S. Mrowka, "A Flat Field Spectrograph for Solar X-Ray Spectroscopy," Proc. Soc. Photo-Opt. Instrum. Eng. **503,** 86 (1984).
12. M. C. Hettrick and S. Bowyer, "Variable Line-Space Gratings: New Designs for Use in Grazing Incidence Spectrometers," Appl. Opt. **22,** 3921 (1983).
13. M. C. Hettrick, "Aberrations of Varied Line-Space Grazing Incidence Gratings in Converging Light Beams," Appl. Opt. **23,** 3221 (1984).
14. M. C. Hettrick and S. Bowyer, "Grazing Incidence Telescopes: a New Design Class for Soft X-Ray and EUV Spectroscopy," Appl. Opt. **23,** 3732 (1984).
15. W. Cash, "X-Ray Spectrographs Using Radial Groove Gratings," Appl. Opt. **22,** 3971 (1983).
16. W. Werner, "X-Ray Efficiencies of Blazed Gratings in Extreme Off-Plane Mountings," Appl. Opt. **16,** 2078 (1977).

17. M. Neviere, D. Maystre, and W. R. Hunter, "Use of Classical and Conical Diffraction Mountings for XUV Gratings," J. Opt. Soc. Am. **68,** 1106 (1978).
18. K. M. Bystricky and T. A. Fritz, "Advanced Circularly Ruled Gratings for General Surface Metrology," Proc. Soc. Photo.-Opt. Instrum. Eng. **429,** 119 (1983).
19. D. L. Windt and W. Cash, "Laboratory Evaluation of Conical Diffraction Spectrographs," Proc. Soc. Photo.-Opt. Instrum. Eng. **503,** 98 (1984).
20. E. G. Loewen, M. Neviere, and D. Maystre, "Grating Efficiency Theory as It Applies to Blazed and Holographic Gratings," Appl. Opt. **16,** 2711 (1977).
21. P. Vincent, M. Neviere, and D. Maystre, "X-Ray Gratings: the GMS Mount," Appl. Opt. **18,** 1780 (1979).
22. M. C. Hettrick, P. Jelinsky, S. Bowyer, and R. F. Malina, "Proposed Design Class of Grazing Incidence Echelle Spectrometers: Critical Analysis and Reevaluation," Appl. Opt. **23,** 4058 (1984).

Meetings Calendar

1985

May

6–7 Electromagnetic Interference Power & System Protection & Control in the Power Industry course, Chicago *Center for Professional Advancement, P.O. Box H, E. Brunswick, N.J. 08816*

6–8 3rd European Conf. on Integrated Optics, Berlin *I. Weber-Zuckarelli, Heinrich-Hertz-Institut Berlin GmbH, Bereich Intergrierte Optik, Einsteinufer 37, D-1000 Berlin, FRG*

6–8 Satellite Geodetic Positioning, Datums & Datum Transformations course, Wash., D.C. *C. Blouin, Geo. Wash. U., Cont. Eng. Ed., Wash., D.C. 20052*

6–9 Practical Microdensitometry/Photodigitizing Sem., Rochester *RIT/T&E Sem. Ctr., One Lomb Memorial Dr., P.O. Box 9887, Rochester, N.Y. 14623*

6–10 Modern Radiometric & Photometric Measurements course, Wash., D.C. *Laser Inst. of Amer., 5151 Monroe St., Ste. 118W, Toledo, Oh. 43623*

6–10 Laser Applications in Materials Processing course, Boston *Laser Inst. of Amer., 5151 Monroe St., Ste. 118W, Toledo, Oh. 43623*

6–10 Measurement of Laser Output Characteristics course, Las Vegas *Eng. Tech., Inc., P.O. Box 8859, Waco, Tex. 76714*

6–17 Optical Science & Engineering course, Tucson *P. Slater, P.O. Box 18667, Tucson, Ariz. 85731*

7–9 Basic Properties of Optical Materials Mtg., Wash., D.C. *A. Feldman, NBS, Bldg. 223, B-328, Wash., D.C., 20234*

9–11 Lasers in Surgery course, Cincinnati *Laser Inst. of Amer., 5151 Monroe St., Ste. 118W, Toledo, Oh. 43623*

12–16 38th Ann. Conf. SPSE, Atlantic City *W. Nebe, E.I. du-Pont de Nemours & Co., Inc., Experimental Station Bldg., 352, Rm. 155, Wilmington, Del. 19898*

14–16 Int. Conf. on Ion & Plasma Assisted Tech., Munich *CEP Consultants Ltd., 26 Albany St., Edinburgh, EH1 3QH, England*

15–19 Digital Image Processing of Earth Observation Sensor Data course, Wash., D.C. *D. Aldridge, Geo. Wash. U., Cont. Eng. Ed., Wash, D.C. 20052*

16–17 Tunable Solid State Lasers course, Arlington *OSA, Mtgs. Dept., 1816 Jefferson Pl., N.W., Wash., D.C. 20036*

19–24 2nd U.S. - Dutch Int. Symp.: Aerosols, Williamsburg *S. Lee, U.S. Coordinator, U.S. Environmental Protection Agency, Res. Triangle Park, N.C. 27711*

20–24 Fiber & Integrated Optics course, Minneapolis *Contd. Ed. Program, Geo. Wash. U., Wash., D.C. 20052*

21–23 5th Optoelectronic Tech. Mtg., Paris *ESI Publications, 12, rue de Seine, 75006 Paris, France*

21–24 **OSA/IEEE Lasers & Electro-Optics Conf.,** Baltimore *OSA Mtgs. Dept., 1816 Jefferson Pl., N.W., Wash., D.C. 20036*

27 AAAS Laser History Symp., Los Angeles *OSA Mtgs. Dept., 1816 Jefferson Pl., N.W., Wash., D.C. 20036*

29–30 Council for Optical Radiation Measurements Ann. Mtg., Gaithersburg *N. Johnson, 3M Ctr., Bldg. 582-1-15, St. Paul, Minn. 55144*

29–30 Electromagnetic Interference Power & System Protection & Control in the Power Industry course, San Mateo *Center for Professional Advancement, P.O. Box H., E. Brunswick, N.J. 08816*

29–31 APS Ann. Mtg. of the Div. of Electron & Atomic Physics, Norman *Central Registration Services, 1700 Asp Ave., Norman, Okla. 73037*

29–1 June Horizons de l'Optique 85 Conf., Besancon *R. Torge, c/o C. Zeiss, Postfach 1369/1380, D-7082 Oberkochen, FRG*

June

9–13 Soc. for Experimental Stress Analysis Spring Mtg., Las Vegas *SESA, 14 Fairfield Dr., Brookfield Ctr., Conn. 06805*

10–13 Short Wavelength Laser Systems course, Dallas *Eng. Tech., Inc., P.O. Box 8859, Waco, Tex. 76714*

10–13 **Int. Lens Design, OSA Tech. Mtg.,** Cherry Hill *OSA Mtgs. Dept., 1816 Jefferson Pl., N.W., Wash., D.C. 20036*

10–14 Fiber & Integrated Optics course, Wash., D.C. *Contd. Ed. Program, Geo. Wash. U., Wash., D.C. 20052*

continued on page 1290